Int. J. Heat Mass Transfer. Vol. 19, pp. 461–470. Pergamon Press 1976. Printed in Great Britain

CONJUGATE HEAT TRANSFER OF CONTINUOUSLY MOVING SURFACES

KIKUJI CHIDA
Faculty of Engineering, Kanagawa University, 3-27-1 Rokkakubashi, Kanagawa-ku, Yokohama, Japan

and

YOSHIRO KATTO
Faculty of Engineering, University of Tokyo, 7-3-1 Hongo, Bunkyo-ku, Tokyo, Japan

(*Received* 7 *July* 1975)

Abstract—Conjugate heat transfer of continuously moving surfaces (flat plate, circular cylinder) is analyzed taking account of heat conduction in the moving solids, and is shown to be completely arranged using the conjugate dimensionless group $[x\lambda_f\rho_f c_f/u_s e^2(\rho_s c_s)^2$ for flat plate, $x\lambda_f\rho_f c_f/u_s R^2(\rho_s c_s)^2$ for cylinder]. Also the effect of the combination of the solid and the fluid is made clear, first by theoretical studies, then by experiments of flat plates in the water.

NOMENCLATURE

a, thermal diffusivity;
b, coordinate normal to the paper;
B, physical properties parameter, $\lambda_f\rho_f c_f/\lambda_s\rho_s c_s$;
c, specific heat;
e, half thickness of flat plate;
f, dimensionless stream function, equation (24);
f_0, function of Pr, equation (46);
F, dimensionless functional relation;
g, gravitational acceleration;
Gr, Grashof number, $g\beta_f\theta_w x^3/\nu_f^2$;
h, local heat-transfer coefficient;
$L_x, L_y, L_z, L_b, L_\varphi$, fundamental dimension of length for x-, y-, z-, b-, φ-direction;
M, fundamental dimension for mass;
Nu, local Nusselt number, hx/λ_f;
Pe, Peclet number, $u_s x/a_f$;
Pr, Prandtl number, ν_f/a_f;
R, radius of cylinder;
Re, Reynolds number, $u_s x/\nu_f$;
t, temperature;
T, fundamental dimension for time;
u, v, velocity component;
u_s, drawing speed of solid body.

Greek symbols

δ, thickness of laminar velocity boundary layer;
δ_f, thickness of laminar temperature boundary layer;
δ_s, temperature penetration depth in solid body;
ζ, z/e or z/R;
η, $y(u_s/\nu_f x)^{\frac{1}{2}}$;
θ, temperature difference from bulk temperature of fluid, $t-t_\infty$;
Θ, fundamental dimension for temperature;
λ, thermal conductivity;
μ, dynamic viscosity;
ν, kinematic viscosity;
ξ, conjugate dimensionless x-coordinate, $x\lambda_f\rho_f c_f/u_s e^2(\rho_s c_s)^2$ or $x\lambda_f\rho_f c_f/u_s R^2(\rho_s c_s)^2$;
ρ, density;
τ, time;
τ_p, time required from stoppage of endless belt driving motor to taking of interference photograph;
φ, azimuthal coordinate of cylindrical coordinates system;
φ, function of x, equation (29);
ϕ, function of x, equation (30);
ψ, stream function.

Subscripts

f, fluid;
s, solid.

1. INTRODUCTION

INVESTIGATIONS on heat transfer of a continuously moving flat plate [1–4] and a circular cylinder [5–13] have been done under various surface conditions, i.e. that the surface temperature is constant, that the surface heat flux is constant, that the moving solid and the fluid are conjugated through surface thermal conditions, etc.

According to general characteristics of conjugate heat-transfer problems [14], in heat transfer of the continuously moving surface under conjugated conditions the combination of physical properties of the moving solid and the surrounding fluid is supposed to play an important role, since this problem is an unsteady one from a viewpoint of the coordinates system fixed to the moving solid. However in previous investigations under conjugated conditions, theoretical analysis has been done neglecting heat conduction in the solid [12] and experiments have been carried out only in the air by drawing glass fibres [5, 6, 9].

First, in this paper, the problem is discussed using vectorial dimensional analysis which distinguishes the

dimensions of length by phases and dimensionless functional relations describing the phenomenon are determined. The numerical solutions for the flat plate and the cylinder, taking account of heat conduction in the solid, are given and arranged using the conjugate dimensionless group [14] and the combination effect of physical properties of both phases is made clear.

Finally, experiments of the flat plate case to demonstrate the combination effect varying flat plate materials (stainless steel, plastic) and fluid (air, water) are described.

2. FORMULATION OF THE PROBLEM

As shown in Fig. 1, an infinite solid body of constant cross section (flat plate of half thickness e, or circular cylinder of radius R) at temperature $t_0(\theta_0 = t_0 - t_\infty)$ is

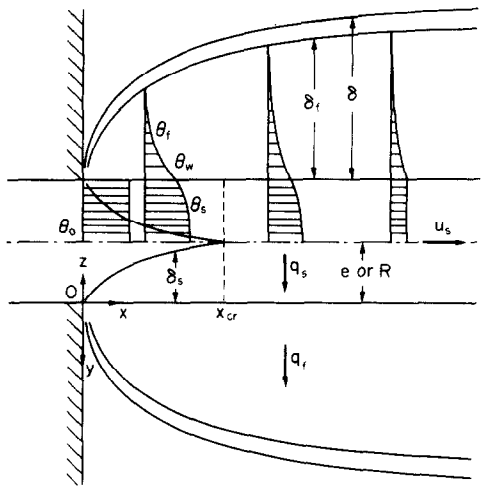

FIG. 1. Conjugate heat transfer of continuously moving solid.

continuously drawn with a constant speed u_s through a drawing slit at $x = 0$ into a fluid whose bulk temperature is $t_\infty(\theta_\infty = 0)$.

This paper deals with conjugate heat transfer of this continuously moving surface, namely heat transfer when the temperature field in the solid and that in the fluid are conjugated to each other through thermal conditions concerning the temperature and the heat flux at the surface, under the assumptions that the fluid is laminar and the drawing speed is fast enough to neglect axial heat conduction.

3. THEORY (VECTORIAL DIMENSIONAL ANALYSIS)

3.1. *Vectorial dimensional analysis* [14]

In this conjugate problem, the solid and the fluid have different physical properties for heat conduction, on the occasion of applying vectorial dimensional analysis to this problem, the z-coordinate must be distinguished from the y-coordinate (as to the coordinates system see Fig. 1), although they have the same spatial direction. As the fundamental dimensions of length, L_x is taken for x-direction, L_y for y-direction, L_z for z-direction and L_b for b-direction.

3.2. *Flat plate*

The whole region is divided into two regions, one from the drawing slit to x_{cr} where the temperature penetration depth in the solid δ_s reaches the centreline of the flat plate, the other from x_{cr} to $x = \infty$. In the first region ($x < x_{cr}$), it must be noted that the half thickness of the flat plate does not concern the phenomenon primarily. The dimensionless functional relation for the surface temperature t_w ($\theta_w = t_w - t_\infty$) is obtained from the following physical quantities (bracketed quantities denote dimensions)

$$\theta_w[\Theta],\quad x[L_x],\quad \mu_f\left[\frac{L_y M}{L_x L_b T}\right],\quad \lambda_f\left[\frac{L_y H}{L_x L_b \Theta T}\right],$$
$$\rho_f\left[\frac{M}{L_x L_y L_b}\right],\quad c_f\left[\frac{H}{M\Theta}\right],\quad \lambda_s\left[\frac{L_z H}{L_x L_b \Theta T}\right],$$
$$\rho_s c_s\left[\frac{H}{L_x L_z L_b \Theta}\right],\quad u_s\left[\frac{L_x}{T}\right],\quad \theta_0[\Theta]$$

by selecting θ_w, μ_f, λ_s as independent quantities:

$$\frac{\theta_w}{\theta_0} = F(B, Pr) \tag{1}$$

where $B(= \lambda_f \rho_f c_f / \lambda_s \rho_s c_s)$ is a parameter representing the combination effect. In the following B will be denoted as "physical properties parameter". In equation (1) it must be noted that the surface temperature of the flat plate keeps a constant value in this region. This means that the fluid in this region takes the similar laminar boundary-layer state. The local heat-transfer coefficient h in this region, therefore, takes the value of the similar laminar boundary layer solution for the constant wall temperature condition h_0. The dimensionless functional relation for the local heat transfer coefficient is thus determined as

$$\frac{Nu_0}{Pe^{\frac{1}{2}}} = \frac{h_0 x}{\lambda_f} \Big/ \left(\frac{u_s x}{a_f}\right)^{\frac{1}{2}} = F(Pr). \tag{2}$$

Dimensionless functional relations for temperature distributions in the fluid and the solid are also obtained as follows:

$$\frac{\theta_f}{\theta_0} = F(\eta, B, Pr) \tag{3}$$

$$\frac{\theta_s}{\theta_0} = F(\zeta^*, B, Pr) \tag{4}$$

where

$$\eta = y\left(\frac{u_s}{\nu_f x}\right)^{\frac{1}{2}},\quad \zeta^* = z\left(\frac{u_s}{a_s x}\right)^{\frac{1}{2}}.$$

In the other region ($x_{cr} < x$), taking account of $e[L_z]$, the following dimensionless functional relations for the surface temperature and the local heat-transfer coefficient are obtained:

$$\frac{\theta_w}{\theta_0} = F(\xi, B, Pr) \tag{5}$$

$$\frac{Nu}{Pe^{\frac{1}{2}}} = F(\xi, B, Pr) \tag{6}$$

where

$$\xi = \frac{x\lambda_f \rho_f c_f}{u_s e^2 (\rho_s c_s)^2} \tag{7}$$

and ξ is a conjugate dimensionless x-coordinate, that is, its definition includes both the conventional dimensionless group defined in the fluid $u_s x/a_f$ and the conventional dimensionless group defined in the solid $a_s x/u_s e^2$. Dimensionless functional relations for temperature distributions in the fluid and the solid are also determined as

$$\frac{\theta_f}{\theta_0} = F(\xi, \eta, B, Pr) \tag{8}$$

$$\frac{\theta_s}{\theta_0} = F(\xi, \zeta, B, Pr) \tag{9}$$

where

$$\zeta = \frac{z}{e}.$$

Thus, when the flat plate with uniform temperature θ_0 at the drawing slit is drawn into the fluid, the surface temperature experiences an abrupt drop at the instance of drawing, and this value is maintained until x_{cr}, then the surface temperature drops continuously as drawing proceeds.

3.3. *Cylinder*

In the neighbourhood of the drawing slit, the situation for the cylinder is the same as for the flat plate. In the cylinder case it must be noted that the radius of the cylinder plays two roles, one as a characteristic length of the cylinder R_s, and the other as a characteristic length of the fluid side coordinate R_f, and the dimensions of the former role is L_z while that of the latter role is L_y. Thus there is no reason to divide regions in the cylinder case as is done in the flat plate case.

The dimensionless functional relation for the surface temperature is determined taking account of physical quantities

$$\theta_w[\Theta],\quad x[L_x],\quad \mu_f\left[\frac{L_y M}{L_x L_\varphi T}\right],\quad \lambda_f\left[\frac{L_y H}{L_x L_\varphi \Theta T}\right],$$

$$\rho_f\left[\frac{M}{L_x L_y L_\varphi}\right],\quad c_f\left[\frac{H}{M\Theta}\right],\quad \lambda_s\left[\frac{L_z H}{L_x L_\varphi \Theta T}\right],$$

$$\rho_s c_s\left[\frac{H}{L_x L_z L_\varphi \Theta}\right],\quad u_s\left[\frac{L_x}{T}\right],\quad R_f[L_y],\quad R_s[L_z],\quad \theta_0[\Theta]$$

as follows:

$$\frac{\theta_w}{\theta_0} = F\left(\xi, \frac{R_f \rho_f c_f}{R_s \rho_s c_s}, B, Pr\right) \tag{10}$$

where ξ is a conjugate dimensionless x-coordinate defined by

$$\xi = \frac{x\lambda_f \rho_f c_f}{u_s R^2 (\rho_s c_s)^2} \tag{11}$$

and the parameter $R_f \rho_f c_f / R_s \rho_s c_s$ is substantially equal to $\rho_f c_f / \rho_s c_s$, the form $\rho_f c_f / \rho_s c_s$ will be used in the following. Also the dimensionless functional relation for the local heat-transfer coefficient is determined as

$$\frac{Nu}{Pe^{\frac{1}{2}}} = F\left(\xi, \frac{\rho_f c_f}{\rho_s c_s}, B, Pr\right). \tag{12}$$

4. THEORY (NUMERICAL SOLUTIONS)

4.1. *Flat plate*

The fundamental equations for the continuously moving flat plate are

$$\frac{\partial u}{\partial x} + \frac{\partial v}{\partial y} = 0 \tag{13}$$

$$u\frac{\partial u}{\partial x} + v\frac{\partial u}{\partial y} = \nu_f \frac{\partial^2 u}{\partial y^2} \tag{14}$$

$$u\frac{\partial \theta_f}{\partial x} + v\frac{\partial \theta_f}{\partial y} = a_f \frac{\partial^2 \theta_f}{\partial y^2} \tag{15}$$

$$u_s \frac{\partial \theta_s}{\partial x} = a_s \frac{\partial^2 \theta_s}{\partial z^2} \tag{16}$$

and relating boundary conditions are

$$\left.\begin{array}{lll} \text{at } y = 0 & u = u_s, & v = 0 \\ \text{at } y = \infty & u = 0 & \end{array}\right\} \tag{17}$$

$$\left.\begin{array}{lll} \text{at } x = 0 & \theta_f = 0, & \theta_s = \theta_0 \\ \text{at } y = 0 (z = 0) & \theta_f = \theta_s, & -\lambda_f \dfrac{\partial \theta_f}{\partial y} = \lambda_s \dfrac{\partial \theta_s}{\partial z} \\ \text{at } y = \infty & \theta_f = 0 & \\ \text{at } z = \mathrm{c} & \dfrac{\partial \theta_s}{\partial z} = 0. & \end{array}\right\} \tag{18}$$

Rewriting fundamental equations and boundary conditions into dimensionless forms following equations and boundary conditions are obtained:

$$\frac{\mathrm{d}^3 f}{\mathrm{d}\eta^3} + \frac{f}{2}\cdot\frac{\mathrm{d}^2 f}{\mathrm{d}\eta^2} = 0 \tag{19}$$

$$\frac{\partial^2}{\partial \eta^2}\left(\frac{\theta_f}{\theta_0}\right) + Pr\cdot\frac{f}{2}\cdot\frac{\partial}{\partial \eta}\left(\frac{\theta_f}{\theta_0}\right) = Pr\cdot\frac{\mathrm{d}f}{\mathrm{d}\eta}\cdot\xi\cdot\frac{\partial}{\partial \xi}\left(\frac{\theta_f}{\theta_0}\right) \tag{20}$$

$$B\cdot\frac{\partial}{\partial \xi}\left(\frac{\theta_s}{\theta_0}\right) = \frac{\partial^2}{\partial \zeta^2}\left(\frac{\theta_s}{\theta_0}\right) \tag{21}$$

and

$$\left.\begin{array}{lll} \text{at } \eta = 0 & \dfrac{\mathrm{d}f}{\mathrm{d}\eta} = 1, & f = 0 \\ \text{at } \eta = \infty & \dfrac{\mathrm{d}f}{\mathrm{d}\eta} = 0 & \end{array}\right\} \tag{22}$$

$$\left.\begin{array}{lll} \text{at } \xi = 0 & \dfrac{\theta_s}{\theta_0} = 1, & \dfrac{\theta_f}{\theta_0} = \dfrac{\theta_{f0}}{\theta_0} \\ \text{at } \eta = 0 (\zeta = 0) & \dfrac{\theta_f}{\theta_0} = \dfrac{\theta_s}{\theta_0}, & \\ & -\dfrac{\partial}{\partial \eta}\left(\dfrac{\theta_f}{\theta_0}\right) = \dfrac{(Pr\cdot\xi)^{\frac{1}{2}}}{B}\cdot\dfrac{\partial}{\partial \zeta}\left(\dfrac{\theta_s}{\theta_0}\right) & \\ \text{at } \eta = \infty & \dfrac{\theta_f}{\theta_0} = 0 & \\ \text{at } \zeta = 1 & \dfrac{\partial}{\partial \zeta}\left(\dfrac{\theta_s}{\theta_0}\right) = 0 & \end{array}\right\} \tag{23}$$

where $f(\eta)$ is the dimensionless stream function defined by

$$f(\eta) = \frac{\psi(x, y)}{(v_f x u_s)^{\frac{1}{2}}} \tag{24}$$

as is done usually. The solution of the energy equation of the fluid for the constant surface temperature condition

$$\frac{d^2}{d\eta^2}\left(\frac{\theta_{f0}}{\theta_0}\right) + Pr \cdot \frac{f}{2} \cdot \frac{d}{d\eta}\left(\frac{\theta_{f0}}{\theta_0}\right) = 0 \tag{25}$$

is taken as the starting temperature condition in the fluid. The numerical solution of equation (19) with boundary conditions equation (22), $f(\eta)$, has been already given by Sakiadis [15]. In this study, equations (20), (21) with boundary conditions equation (23) are simultaneously solved using Sakiadis' solution $f(\eta)$.

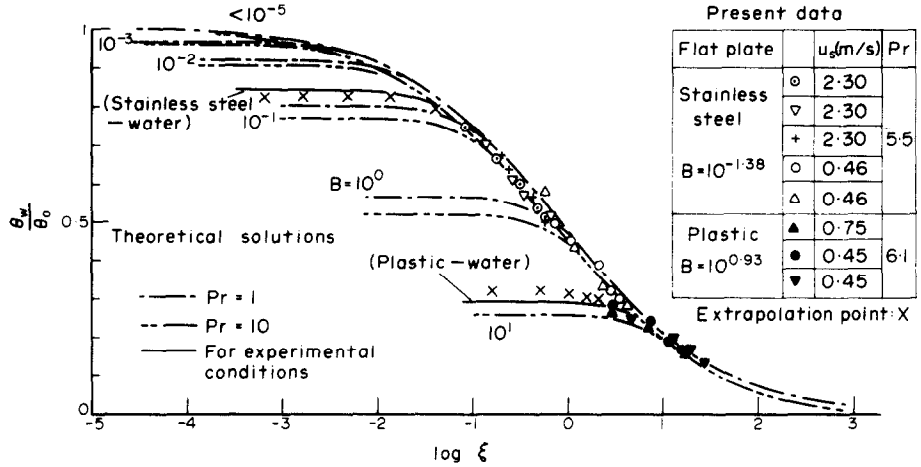

FIG. 2. Surface temperature of continuously moving flat plate.

Numerical calculations are carried out as follows. The whole region including both the fluid and the solid are divided into the grid. Along the x-coordinate lines of the grid are numbered as $i = 1, 2, \ldots$, and so on, along the z-coordinate as $j = 1, 2, \ldots, j_n$ starting from the centre-line of the flat plate (number j_n denotes the surface) and along the y-coordinate as $j = j_n + 1, j_n + 2, \ldots, j_{\max}$. When temperature distributions at any axial position $i, \theta_s(T_{ij}, j = 1, \ldots, j_n)$ and $\theta_f(T_{ij}, j = j_n, \ldots, j_{\max})$, are known, the temperature distribution at the axial position $i+1 (T_{i+1j}, j = 1, \ldots, j_n, \ldots, j_{\max})$ is determined by equations (20), (21) with boundary conditions equation (23) in finite difference forms, as the solution of $j_{\max}$-dimensional linear equations. Calculation results for the surface temperature are given in Fig. 2 as theoretical solutions.

4.2. *Cylinder*

It is difficult to solve fundamental equations for cylinder in partial differential forms, here the problem is solved using the integral method, the same method used by Bourne and Dixon [12]. They neglected heat conduction in the cylinder, and could not detect the combination effect. In this study, heat conduction in z-direction in the cylinder is taken account of.

Fundamental equations of integrated forms are

$$\frac{d}{dx}\int_0^{\delta} u^2 \cdot (R+y) \cdot dy + R \cdot v_f \cdot \left(\frac{\partial u}{\partial y}\right)_{y=0} = 0 \tag{26}$$

$$\frac{d}{dx}\int_0^{\delta_f} u \cdot \theta_f \cdot (R+y) \cdot dy + R \cdot a_f \cdot \left(\frac{\partial \theta_f}{\partial y}\right)_{y=0} = 0 \tag{27}$$

$$\frac{d}{dx}\int_0^{R} u_s \cdot \theta_s \cdot (R-z) \cdot dZ + R \cdot a_s \cdot \left(\frac{\partial \theta_s}{\partial z}\right)_{z=0} = 0 \tag{28}$$

where δ, δ_f are velocity and temperature boundary-layer thicknesses respectively. The velocity profile is put in the form

$$\frac{u}{u_s} = 1 - \frac{1}{\varphi} \cdot \ln\left(1 + \frac{y}{R}\right) \tag{29}$$

and the temperature profile in the fluid

$$\frac{\theta_f}{\theta_w} = 1 - \frac{1}{\phi} \cdot \ln\left(1 + \frac{y}{R}\right) \tag{30}$$

where φ and ϕ are unknown functions of x. On the other hand, the temperature profile of the cylinder in the region $x < x_{cr}$ is expressed in the form

$$\frac{\theta_s - \theta_0}{\theta_w - \theta_0} = 1 - 2 \cdot \left(\frac{z}{\delta_s}\right) + \left(\frac{z}{\delta_s}\right)^2 \tag{31}$$

using boundary conditions

$$\begin{aligned} &\text{at } z = 0 \qquad \theta_s = \theta_w \\ &\text{at } z = \delta_s \qquad \theta_s = \theta_0, \quad \frac{\partial \theta_s}{\partial z} = 0 \end{aligned} \tag{32}$$

and in this region there exists one more condition, i.e. $q_{wf} = q_{ws}$, and this condition can be expressed by θ_w, ϕ, δ_s as

$$\frac{\delta_s}{R} = 2 \cdot \phi \cdot \frac{\lambda_s}{\lambda_f} \cdot \frac{\theta_0 - \theta_w}{\theta_w} \tag{33}$$

In the region $x > x_{cr}$, the temperature profile is determined as

$$\frac{\theta_s}{\theta_w} = 1 + \frac{\lambda_f}{\lambda_s \phi} \cdot \left(\frac{z}{R}\right) - \frac{1}{2} \cdot \frac{\lambda_f}{\lambda_s \phi} \cdot \left(\frac{z}{R}\right)^2 \tag{34}$$

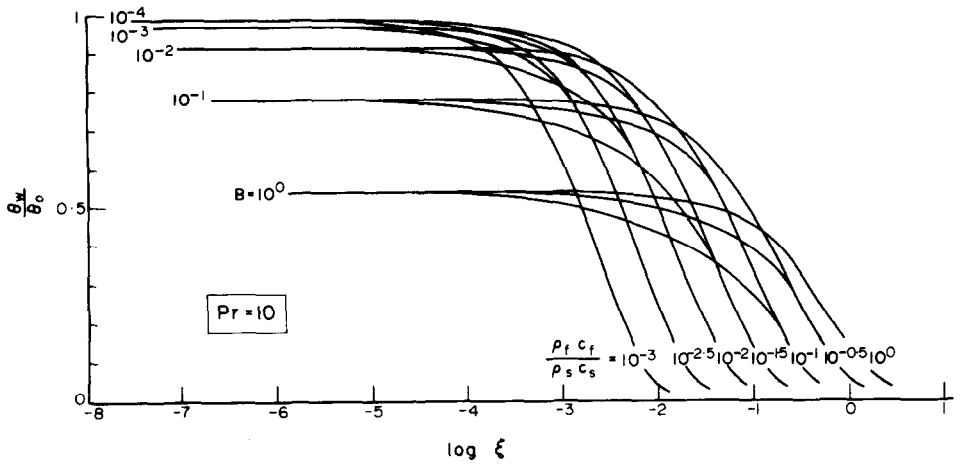

FIG. 3. Surface temperature of continuously moving cylinder.

using conditions

$$\text{at } z=0 \qquad \theta_s=\theta_w, \quad q_{wf}=q_{ws}$$
$$\text{at } z=R \qquad \frac{\partial\theta_s}{\partial z}=0. \tag{35}$$

Putting equation (29) into equation (26) and rearranging, the momentum equation takes the form

$$\frac{d\xi}{d\varphi}=\frac{1}{2Pr}\cdot\left(\frac{\rho_f c_f}{\rho_s c_s}\right)^2\cdot\frac{e^{2\varphi}\cdot(\varphi-1)+\varphi+1}{\varphi^2}. \tag{36}$$

The energy equation for the fluid can be converted into the following form, inserting equations (29) and (30) into equation (27),

$$\frac{d}{d\varphi}\left[\frac{\left(\frac{\theta_w}{\theta_0}\right)}{\varphi\phi}\cdot\{e^{2\phi}\cdot(\varphi-\phi+1)-(2\varphi\phi+\varphi+\phi+1)\}\right]$$
$$=\frac{2\left(\frac{\theta_w}{\theta_0}\right)}{Pr}\cdot\frac{e^{2\varphi}\cdot(\varphi-1)+\varphi+1}{\varphi^2\phi} \quad (\delta>\delta_f) \tag{37}$$

$$\frac{d}{d\varphi}\left[\frac{\left(\frac{\theta_w}{\theta_0}\right)}{\varphi\phi}\cdot\{e^{2\varphi}\cdot(\phi-\varphi+1)-(2\varphi\phi+\varphi+\phi+1)\}\right]$$
$$=\frac{2\left(\frac{\theta_w}{\theta_0}\right)}{Pr}\cdot\frac{e^{2\varphi}\cdot(\varphi-1)+\varphi+1}{\varphi^2\phi} \quad (\delta<\delta_f). \tag{38}$$

The energy equation for the cylinder, equation (28), is transformed into

$$\frac{d}{d\varphi}\left[\left\{1-\frac{1-\left(\frac{\theta_w}{\theta_0}\right)}{2\cdot\left(\frac{\theta_w}{\theta_0}\right)}\cdot\frac{\lambda_s\phi}{\lambda_f}\right\}\cdot\frac{\left\{1-\left(\frac{\theta_w}{\theta_0}\right)\right\}^2}{\left(\frac{\theta_w}{\theta_0}\right)}\cdot\frac{\lambda_s\phi}{\lambda_f}\right]$$
$$=\frac{3\cdot\left(\frac{\theta_w}{\theta_0}\right)}{4\cdot Pr}\cdot\left(\frac{\rho_f c_f}{\rho_s c_s}\right)\cdot\frac{e^{2\varphi}\cdot(\varphi-1)+\varphi+1}{\varphi^2\phi} \tag{39}$$

in the region $x<x_{cr}$ using equation (31) and

$$\frac{d}{d\varphi}\left\{\left(1+\frac{\lambda_f}{4\lambda_s\phi}\right)\cdot\left(\frac{\theta_w}{\theta_0}\right)\right\}$$
$$=-\frac{\left(\frac{\theta_w}{\theta_0}\right)}{Pr}\cdot\left(\frac{\rho_f c_f}{\rho_s c_s}\right)\cdot\frac{e^{2\varphi}\cdot(\varphi-1)+\varphi+1}{\varphi^2\phi} \tag{40}$$

in the region $x>x_{cr}$ using equation (34).

Numerical calculations are carried out as follows. First, integration of equation (36) gives the relation between ξ and φ. Then the energy equation for the fluid and the energy equation for the cylinder are simultaneously solved concerning unknowns θ_w/θ_0 and ϕ as functions of φ, and through the relation between ξ and φ, solutions are converted to relations θ_w/θ_0 vs ξ and ϕ vs ξ. The relation ϕ vs ξ is finally arranged as the relation $Nu/Pe^{\frac{1}{2}}$ vs ξ using

$$\frac{Nu}{Pe^{\frac{1}{2}}}=\left(\frac{\rho_s c_s}{\rho_f c_f}\right)\cdot\frac{\xi^{\frac{1}{2}}}{\phi}. \tag{41}$$

In Fig. 3, the surface temperature variation with ξ are shown for $Pr=10$.

4.3. *Considerations on the theoretical results*

Vectorial dimensional analysis shows that the moving solid experiences a sudden drop of the surface temperature at the neighbourhood of the drawing slit, under the assumptions stated in Section 2, and the temperature is determined by the flow condition and the combination of the fluid properties and the solid properties. Numerical calculation results shown in Figs. 2 and 3 confirm this situation.

As a preparation, the classical contact problem of unsteady heat conduction is considered. Two half-infinite bodies at different temperatures (t_{0f} in f-phase, t_{0s} in s-phase) are suddenly brought into contact at time $\tau=0$. According to the textbook on heat conduction [16], the temperature of the boundary surface $\theta_w(=t_w-t_{0f})$ is kept constant during whole process

$\tau > 0$, and the value is given as follows ($\theta_0 = t_{0s} - t_{0f}$)

$$\frac{\theta_w}{\theta_0} = \frac{\lambda_s a_s^{-\frac{1}{2}}}{\lambda_s a_s^{-\frac{1}{2}} + \lambda_f a_f^{-\frac{1}{2}}}. \tag{42}$$

This equation can be rewritten using B as

$$\frac{\theta_w}{\theta_0} = \frac{1}{1+B^{\frac{1}{2}}}. \tag{43}$$

Now we return to our problem. As stated in the Section 3, near the drawing slit the dimension e does not concern the phenomenon primarily, the solid in this region can be considered to be half-infinite. If the problem is seen from the viewpoint of the coordinates system fixed to the moving solid, the problem is similar to the above described unsteady contact problem, only differing in that there exists the laminar flow in the fluid. The classical theory states that the temperature distribution in the half-infinite solid is

$$\frac{\theta_s - \theta_w}{\theta_0 - \theta_w} = \operatorname{erf}\left(\frac{z}{2\sqrt{(a_s \tau)}}\right) \tag{44}$$

and the surface heat flux calculated from this equation is

$$q_{ws} = \frac{\lambda_s(\theta_0 - \theta_w)}{\sqrt{(\pi a_s \tau)}}. \tag{45}$$

On the other hand, as the fluid is in the state of the similar laminar boundary layer with the constant surface temperature, heat transfer can be expressed by

$$\frac{Nu_0}{Pe^{\frac{1}{2}}} = f_0 \tag{46}$$

where f_0 is a function of Pr only and $f_0 = 0.4174$, $0.4438, 0.5314, \ldots$, according to $Pr = 0.7, 1, 10, \ldots$ [1]. Equation (46) gives the surface heat flux calculated from the fluid side:

$$q_{wf} = f_0 \cdot \lambda_f \cdot \sqrt{\left(\frac{u_s}{a_f x}\right)} \cdot \theta_w. \tag{47}$$

As the drawing speed u_s is constant, dependency of q_{ws} and q_{wf} on x are equal, and putting $q_{ws} = q_{wf}$ the following formula is obtained:

$$\frac{\theta_w}{\theta_0} = \frac{1}{1+B^{\frac{1}{2}} \cdot \sqrt{\pi} \cdot f_0}. \tag{48}$$

The values calculated by equation (48) coincide with numerical solutions shown in Fig. 2 and Fig. 3. It must be also noted that equation (48) coincide with equation (43) when the fluid becomes still relative to the solid, i.e. when $Pr \to \infty$.

5. EXPERIMENT

In this chapter, experiments to check theoretical results, especially the effect of the physical properties parameter, varying combinations of fluids (air, water) and flat plates (stainless steel, plastic), are described.

The experiments are limited to the flat plate case, since the effect of the physical properties parameter on the cylinder case is much the same, and as to the cylinder case only a comparison between theoretical results and the presently available data which are arranged using the conjugate dimensionless x-coordinate is made.

5.1. *Experimental apparatus*

There are at least two ways to realize the flow of the continuously moving flat plate in the laboratory, one to use a large diameter drum such as used by Tsou *et al.* [1], the other to use an endless belt or a very long belt. In this study, endless belts of 4–4.5 m long and 4 cm wide are used. The driving system of the endless belt is shown in Fig. 4. The motor, through

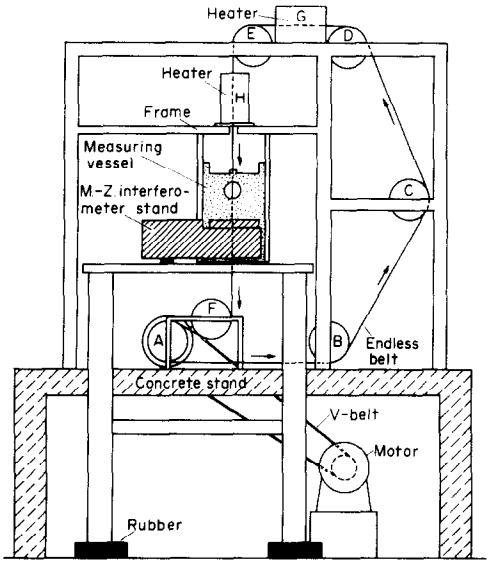

FIG. 4. Experimental apparatus.

the pulley A, drives the endless belt with speed u_s from 0.45 to 3.0 m/s. The pulley C can be slid horizontally and gives the tension to the endless belt. Cylindrical heaters G and H can heat the endless belt with variable heating rate. The measuring section is the circular window region positioned at the upper part of the measuring vessel fitted to the frame. The measuring vessel (260 × 200 × 70 mm) is composed of two half-vessels and assembled holding the endless belt between them.

The velocity distribution in the air is measured by the constant-temperature type hot anemometer (tungsten hot wire of 5 μ dia.). Temperatures in the fluid are measured by the Mach–Zehnder interferometer (6 cm dia.).

5.2. *Measuring principle of surface temperature in water experiments*

In air experiments, temperature boundary layers are thick enough that displacements of fringes in interference photographs give temperature distributions through the relation

$$\theta_f = \frac{\Delta s}{\Delta s_d} \cdot \frac{\lambda_w}{L} \cdot \frac{1}{\left(\frac{dn}{dt_f}\right)} \tag{49}$$

where L is the width of the endless belt, n is the refractive index of the fluid, λ_w is the wave length of the monochromatic light, Δs_d is the distance between neighbouring reference fringes and Δs is the fringe

displacement from the reference fringe at an arbitrary position y (see Fig. 5). However in water experiments, temperature boundary layers are quite thin and almost

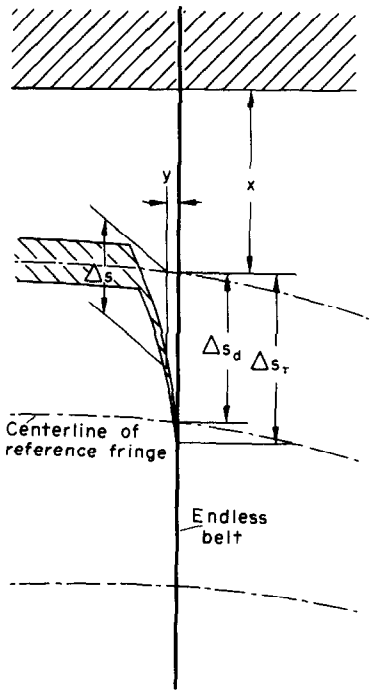

FIG. 5. Schematic representation of interference photograph.

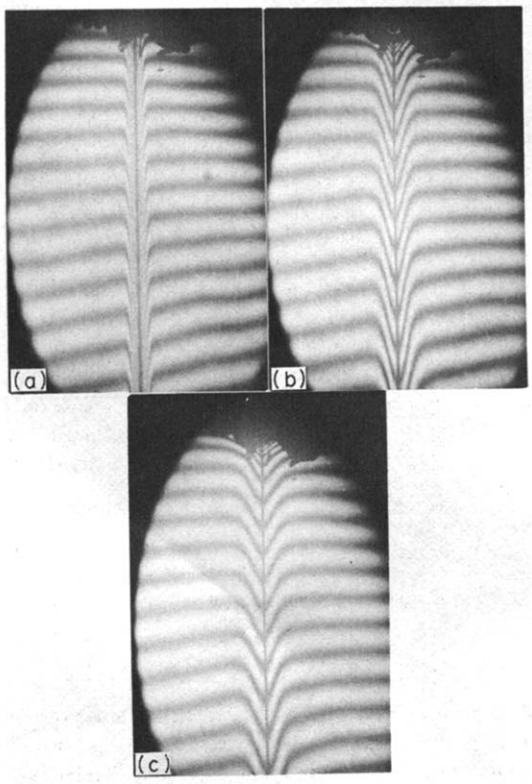

FIG. 6. Unsteady process in water after stoppage of endless belt driving motor.

cannot be seen, so temperature distributions in the water when the endless belt is moving cannot be obtained. Therefore a following method to determine surface temperatures is employed in this study.

After the endless belt driving motor is suddenly made to stop at time $\tau = 0$, the surface temperature of the endless belt begins to propagate into the water. In Fig. 6, interference photographs after the stoppage of the endless belt driving motor are shown in order of time passage. It can be easily seen that for a short time after the stoppage of the endless belt driving motor, unsteady heat conduction into the water occurs normal to the endless belt surface [the first stage, see Fig. 6(a)], then rises heat conduction parallel to the endless belt surface and/or natural convection [see Fig. 6(b), (c)]. We notice the first stage of this propagation process. In Fig. 6(a) the situation is not clear because of over-heating of the endless belt, so thereafter the heating rate of the endless belt is appropriately adjusted. One of interference photographs of the first stage thus obtained is shown in Fig. 7. Figure 5 represents the schematic diagram of the interference photograph. In the following, the temperature variation with time at a fixed axial position x (see Fig. 5) is discussed. From time $\tau = 0$ to time $\tau = \tau_p$ when the interference photograph is taken, the temperature at $(x, y) = (x, 0)$ falls gradually from the initial value $\theta_w(x)$ to $\theta_\tau(\tau_p)$. If τ_p is not so large (in our experiments, $\tau_p = 0.5$–1.0 s) the nose part of the temperature propagation will keep the initial characteristics, since the

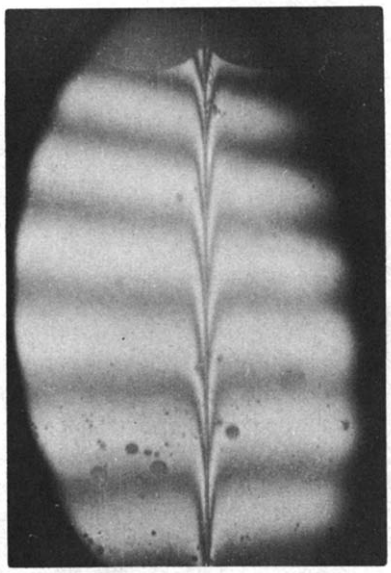

FIG. 7. Example of interference photograph of one-dimensional unsteady heat conduction in water.

temperature change, $\theta_\tau(\tau) - \theta_w$, propagates into the water following after the initial temperature propagation. To confirm this situation, calculations of unsteady one-dimensional heat conduction are done, giving the initial temperature distribution in the boundary layer formed when the endless belt is continuously moving (the thickness of the temperature boundary

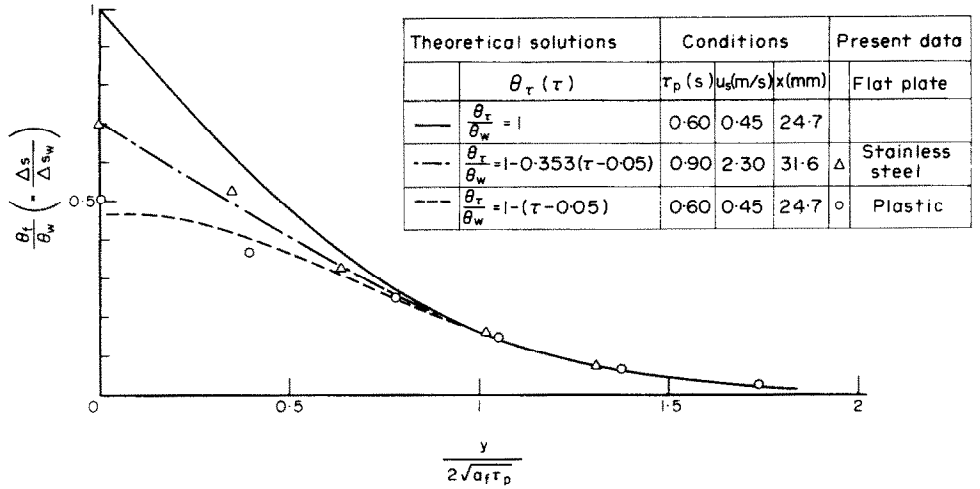

FIG. 8. One-dimensional unsteady heat conduction in water.

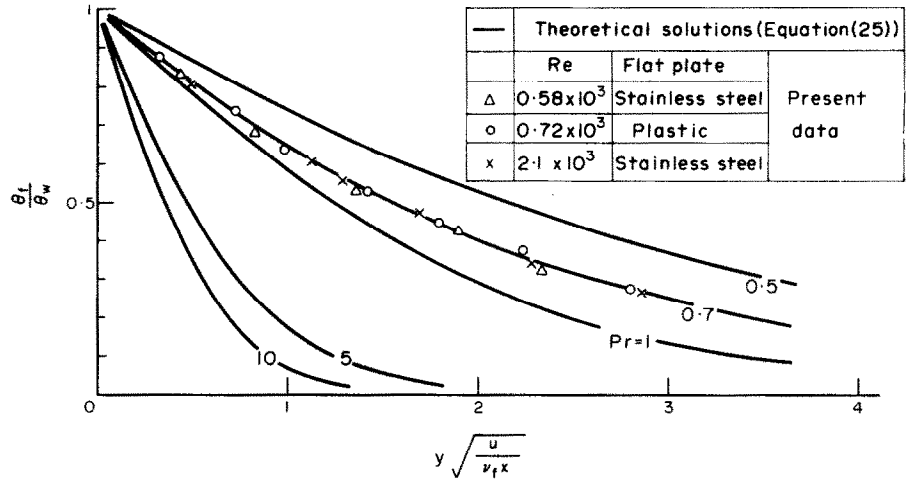

FIG. 9. Temperature distribution in air.

layer is very thin, as already stated), and the temperature variation at $(x, 0)$ with time in three ways, $\theta_\tau/\theta_w = 1$, $\theta_\tau/\theta_w = 1-0.353(\tau-0.05)$ and $\theta_\tau/\theta_w = 1-(\tau-0.05)$. Calculated temperature distributions in the water at time τ_p are shown in Fig. 8. These results show that the initial temperature distribution does not affect this unsteady heat conduction process, and that the nose part of the temperature propagation ($\theta_f/\theta_w <$ 0.25 in Fig. 8) coincide with each other irrespective of differences of given variation ways of the temperature with time, and they can be represented by the curve $\mathrm{erfc}[y/2\sqrt{(a_f\tau)}]$. Thus the surface temperature θ_w at the axial position x can be obtained by plotting the nose part data derived from the interference photograph on the curve $\mathrm{erfc}[y/2\sqrt{(a_f\tau)}]$. Some experimental data are also plotted in Fig. 8.

5.3. *Flat plate results*

Experiments in the air are substantially same to experiments with the constant surface temperature, since the values of the physical properties parameter are less than 10^{-4} for both the stainless steel endless belt and the plastic endless belt, and the measurable length of x is less than 4 cm, therefore experiments in the air are to be done in the neighbourhood of the first region described in the Section 3.2 (see theoretical solutions in Fig. 2). Temperature distributions by air experiments are shown in Fig. 9. By these results it is seen that the laminar boundary layer with constant surface temperature [see equation (25)] is formed on the continuously moving endless belt.

Surface temperatures of the continuously moving endless belt in water experiments are shown in Fig. 2 using $\log_{10}\xi$. Figure 2 is constructed by the following procedure. From one interference photograph as shown in Fig. 7, θ_w for three to five points of x can be obtained by the method described in the preceding section. However θ_0 cannot be measured in our experiments, so one value of θ_w for an arbitrary point x is first put on the theoretical curve, then the reading of the ordinate readily gives the value of θ_0. Using thus determined value of θ_0, θ_w for other points are plotted on Fig. 2. Extrapolation points in Fig. 2 are derived by plotting θ_w/θ_0 vs ξ directly.

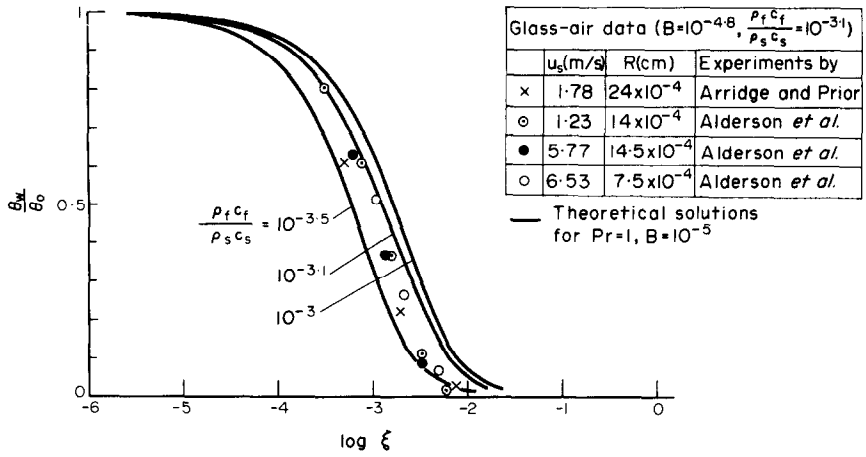

FIG. 10. Arrangement of presently available data for continuously moving cylinder.

5.4. *Discussions on flat plate experiments*

In this section several discussions concerning flat plate experiments are made.

Concerning two-dimensionality of the endless belts it seems to be no matter, since thicknesses of boundary layers formed on the endless belts are very thin.

Finiteness of the measuring vessel usually gives rise to useless secondary flow disturbances such as a circulation, but in our experiments steady states are quickly realized after commencement of the endless belts driving, therefore measurements can be made in short times, within which there can be seen no disturbances in interference fringes.

Also disturbances resulting from natural convection are not observed, and for the sake of smallness of temperature differences between the endless belts and fluids, values of Gr/Re^2 are less than 4×10^{-2} in air experiments and less than 10^{-4} in water experiments.

Lastly, in interference photographs taken in water experiments reference fringes are slightly curved and distances between them are not uniform. Reasons for these deformations are probably due to deformations of optical glasses attached to windows of the measuring vessel and the compensating vessel. However corrections owing to this are negligibly small.

5.5. *Arrangement of presently available cylinder data*

Presently available cylinder data for conjugate heat transfer are those of glass fibers drawn into the air [5, 6, 9]. Data taken from [12] (in [12], data from [6] and [9] are cited), arranged using the conjugate dimensionless x-coordinate, equation (11), are plotted in Fig. 10. Because of lack of physical properties data for glasses under experimental conditions, use is made of physical properties data for the quartz glass at 20°C.

6. CONCLUDING REMARKS

Conjugate heat transfer of the continuously moving surface (flat plate, cylinder) is discussed taking account of heat conduction in the solid. Through theoretical studies and experiments using the Mach–Zehnder interferometer, it is shown that this problem is completely arranged by using the conjugate dimensionless x-coordinate, and the physical properties parameter B which represents the effect of the combination of the solid and fluid physical properties on heat transfer is also shown to play an important role in this heat transfer.

REFERENCES

1. F. K. Tsou, E. M. Sparrow and R. J. Goldstein, Flow and heat transfer in the boundary layer on a continuously moving surface, *Int. J. Heat Mass Transfer* **10**, 219–234 (1967).
2. L. E. Erickson, L. T. Fan and V. G. Fox, Heat and mass transfer on a moving continuous flat plate with suction or injection, *I/EC Fundamentals* **5**, 19–25 (1966).
3. J. F. Griffin and J. L. Throne, On thermal boundary layer growth on continuous moving belts, *A.I.Ch.E. Jl* **13**, 1210–1211 (1967).
4. G. Horvay, Temperature distribution in a slab moving from a chamber at one temperature to a chamber at another temperature, *J. Heat Transfer* **83**, 391–402 (1961).
5. O. L. Anderson, Cooling time of strong glass fibers, *J. Appl. Phys.* **29**, 9–12 (1958).
6. R. G. C. Arridge and K. Prior, Cooling time of silica fibres, *Nature, Lond.* **203**, 386–387 (1964).
7. R. M. Griffith, Velocity, temperature and concentration distributions during fiber spinning, *I/EC Fundamentals* **3**, 245–250 (1964).
8. L. R. Glicksman, The cooling of glass fibres, *Glass Technol.* **9**, 131–138 (1968).
9. J. V. Alderson, J. B. Caress and R. L. Sager, The cooling rate of a glass fibre in the continuous filament process, Laboratory report No. L.R. 235 of Pilkington Bros. Ltd., Lathom, Lancashire (1968).
10. G. Vasudevan and S. Middleman, Momentum, heat and mass transfer to a continuous cylindrical surface in axial motion, *A.I.Ch.E. Jl* **16**, 614–619 (1970).
11. D. E. Bourne and D. G. Elliston, Heat transfer through the axially symmetric boundary layer on a moving circular fibre, *Int. J. Heat Mass Transfer* **13**, 583–593 (1970).
12. D. E. Bourne and H. Dixon, The cooling of fibres in the formation process, *Int. J. Heat Mass Transfer* **24**, 1323–1331 (1971).
13. G. Horvay and M. Dacosta, Temperature distribution in a cylindrical rod moving from a chamber at one temperature to a chamber at another temperature, *J. Heat Transfer* **86**, 265–270 (1964).

14. K. Chida and Y. Katto, Study on conjugate heat transfer by vectorial dimensional analysis, *Int. J. Heat Mass Transfer* **19**(5), 453–460 (1976).
15. B. C. Sakiadis, Boundary layer behaviour on continuous solid surfaces—II. The boundary layer on a continuous flat surface, *A.I.Ch.E. Jl* **7**, 221–225 (1961).
16. H. S. Carslaw and J. C. Jaeger, *Conduction of Heat in Solids*, p. 88. Clarendon Press, Oxford (1959).

TRANSFERT DE CHALEUR CONJUGUE SUR DES SURFACES EN MOUVEMENT CONTINU

Résumé—On étudie le transfert de chaleur conjugué sur des surfaces en mouvement continu (plaque plane, cylindre circulaire) en tenant compte de la conduction thermique dans les solides en mouvement, et on montre qu'il peut être traité complètement à l'aide du groupement adimensionnel conjugué [$X\lambda_f\rho_f C_f/U_S\rho^2\ (\rho_S C_S)^2$ pour la plaque plane, $X\lambda_f\rho_f C_f/U_S R^2\ (\rho_S C_S)^2$ pour le cylindre]. L'effet de l'association du solide et du fluide est également éclairci, d'abord par des études théoriques, ensuite par des expériences sur plaques planes dans l'eau.

ZUSAMMENGESETZTER WÄRMEÜBERGANG AN GLEICHMÄSSIG BEWEGTEN OBERFLÄCHEN

Zusammenfassung—Der zusammengesetzte Wärmeübergang an gleichmässig bewegten Oberflächen (ebene Platte, kreisförmiger Zylinder) wird analysiert unter Berücksichtigung der Wärmeleitung im bewegten Festkörper und wird vollständig dargestellt durch folgende dimensionslose Gruppen,

$X\lambda_f\rho_f C_f/U_s e^2\ (\rho_s C_s)^2$ für die ebene Platte

$X\lambda_f\rho_f C_f/U_s R^2\ (\rho_s C_s)^2$ für den Zylinder

Auch der Einfluß der Kombination von Festkörper und Fluid wird dargelegt, sowohl durch theoretische Untersuchungen wie auch durch Versuche mit ebenen Platten in Wasser.

СОПРЯЖЕННЫЙ ТЕПЛООБМЕН НЕПРЕРЫВНО ДВИЖУЩИХСЯ ПОВЕРХНОСТЕЙ

Аннотация — Анализируется сопряженный теплообмен непрерывно движущихся поверхностей (плоская пластина, круговой цилиндр) с учетом теплопроводности в движущихся твердых телах. Показано, что сопряженный теплообмен описывается с помощью безразмерного комплекса [$X\lambda_f\rho_f c_f/u_s e^2(\rho_s c_s)^2$ для плоской пластины и $X\lambda_f\rho_f c_f/u_s R^2(\rho_s c_s)^2$ для цилиндра]. Кроме того, теоретически и экспериментально на примере плоских пластин в воде исследован эффект взаимодействия твердого тела и жидкости.